

# Pathways to turbulence from internal waves in a stratified horizontally sheared flow

By S. F. Lewin<sup>†</sup>, A. Balakrishna AND M. M. P. Couchman<sup>‡</sup>

We consider a series of direct numerical simulations capturing the turbulent transition resulting from the interaction of a propagating internal gravity wave with a horizontal shear layer in a fluid with uniform vertical stratification. Two distinct mechanisms influencing the turbulent transition are highlighted: convective-like instability due to wave trapping within the shear layer and vertical shear instability due to the advection of momentum by the wave across the shear layer. The relative importance of these mechanisms may be controlled by varying the streamwise wave number and the strength of the background stratification, forming the parameter space considered here. Characteristic differences in the turbulent state and the resulting mixing of the density field are revealed through an analysis of key turbulent statistics and energy budgets.

---

## 1. Introduction

Away from boundaries with the atmosphere, sea ice and the solid earth, the ocean is stably stratified by density. This enables the existence of a continuum of internal gravity waves with spatial scales of tens of kilometers down to meters, playing a significant role in the transport and distribution of energy and momentum throughout the ocean interior (Garrett & Munk 1979). The means by which these waves break and dissipate their energy via small-scale turbulence is of particular interest because the resulting vertical mixing of heat and other scalars is a key process influencing the global overturning circulation (Waterhouse *et al.* 2014). In the absence of planetary rotation, much of the existing literature on wave breaking has focused on vertical shear layers, which, for example, focus incoming internal wave energy at critical levels leading to breaking (Booker & Bretherton 1967) or may themselves represent a section of a larger wave that becomes locally unstable according to a relevant stability criterion (Miles 1961; Howard 1961). While scenarios dominated by a horizontal rather than vertical component of shear have received relatively less attention, they have nonetheless been demonstrated to be capable of exhibiting significant turbulence production, both in isolation and through interaction with internal waves (Jacobitz & Sarkar 1998; Staquet & Huerre 2002).

Recently, Lewin & Caulfield (2024) showed that the addition of wave-like perturbations to a horizontal shear layer could induce a transition to turbulence that was otherwise precluded in the system, highlighting the importance of internal wave and vertical vorticity interactions in modifying the stability and subsequent turbulent properties of strongly stratified flows. Motivated by their study, we consider here the more general problem of a monochromatic internal wave packet incident on a horizontal shear layer. The primary goal is to study the nonlinear evolution of the system following the expected transient growth of wave energy due to interaction with the background shear and to

<sup>†</sup> Department of Mechanical Engineering, University of California, Berkeley

<sup>‡</sup> Department of Mathematics and Statistics, York University, Canada

characterize the subsequent dynamics in terms of dimensionless parameters describing the shear, stratification and incident wave. We focus on cases where energy growth results in turbulence production, rather than other phenomena such as wave reflection or viscous damping. Particular attention is given to understanding how the energy pathways sustaining turbulence are modified by the variable interactions between the wave and horizontal shear.

In Section 2, we describe the problem setup and briefly outline the linear theory governing the limiting behaviors of the system. Results from a series of eight direct numerical simulations are presented and discussed in Section 3. Finally, in Section 4, we discuss wider implications and future avenues of investigation.

## 2. Problem formulation

### 2.1. Setup

We consider a horizontal shear layer in a channel  $\mathbf{x} \in [-2\pi, 2\pi] \times [-2\pi, 2\pi] \times [0, 2\pi]$  that is periodic in  $x$  and  $z$  and wall-bounded in  $y$ . Stratification is imposed by assuming a linear background density gradient in  $z$ . The dynamics are modeled using the nondimensional Boussinesq equations for the velocity field  $\mathbf{u} = (u, v, w)$  alongside buoyancy ( $b$ ) and pressure ( $p$ ) perturbations away from the background hydrostatic equilibrium:

$$\frac{D\mathbf{u}}{Dt} = -\nabla p + Ri b\hat{\mathbf{z}} + \frac{1}{Re} \nabla^2 \mathbf{u}, \quad (2.1)$$

$$\nabla \cdot \mathbf{u} = 0, \quad (2.2)$$

$$\frac{Db}{Dt} = -w + \frac{1}{RePr} \nabla^2 b. \quad (2.3)$$

Using asterisks to denote dimensional quantities,  $\mathbf{u}$ ,  $\mathbf{x}$  and  $t$  are nondimensionalized using the velocity and length scales  $U^*$  and  $L^*$  associated with the shear layer (note in particular that time is nondimensionalized with the advective timescale  $L^*/U^*$ ), whilst  $b$  is nondimensionalized by  $N^{*2}L^*$ , where  $N^*$  is the buoyancy frequency associated with the background stratification. Here,  $Re = U^*L^*/\nu^*$  and  $Pr = \nu^*/\kappa^*$  are the Reynolds and Prandtl numbers, and  $Ri = N^{*2}L^{*2}/U^{*2}$  is the Richardson number describing the relative importance of buoyancy and inertial forces from the stratification and shear.

As initial conditions, a monochromatic internal wave packet (attenuated in  $y$ ) is superposed on a horizontally sheared flow

$$\mathbf{u}(\mathbf{x}, t = 0) = \mathbf{u}_S + \mathbf{u}_{IW} e^{-(y+2)^2/a^2}, \quad b(\mathbf{x}, t = 0) = b_{IW} e^{-(y+2)^2/a^2}, \quad (2.4)$$

where subscripts  $S$  and  $IW$  denote shear and internal wave components, respectively. We take

$$\mathbf{u}_S = \tanh(y)\mathbf{e}_x, \quad (2.5)$$

whilst the internal wave perturbations with wave vector  $\mathbf{k} = (k_x, k_y, k_z)$  are given by real parts of the relevant polarization relations

$$\begin{aligned} b_{IW} &= \frac{s}{k_z} \exp(i\mathbf{k} \cdot \mathbf{x}), & u_{IW} &= -\frac{isRik_x}{\omega|\mathbf{k}|^2} \exp(i\mathbf{k} \cdot \mathbf{x}), \\ v_{IW} &= -\frac{isRik_y}{\omega|\mathbf{k}|^2} \exp(i\mathbf{k} \cdot \mathbf{x}), & w_{IW} &= \frac{is\omega}{k_z} \exp(i\mathbf{k} \cdot \mathbf{x}). \end{aligned} \quad (2.6)$$

Here,  $\omega$  is the wave frequency satisfying the dispersion relation  $\omega^2 = Ri(k_x^2 + k_y^2)/|\mathbf{k}|^2$ ,

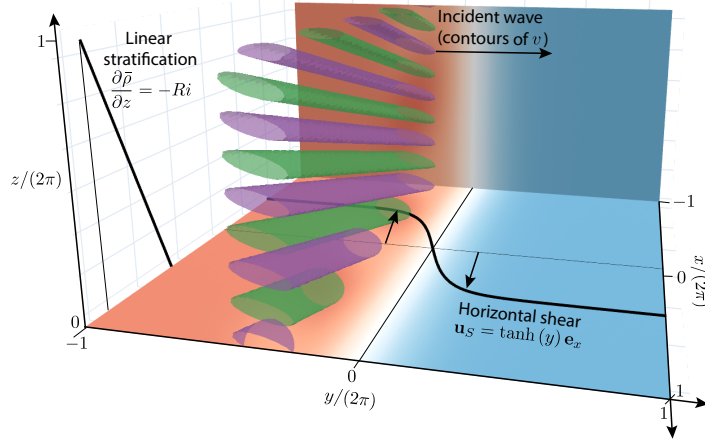


FIGURE 1. A schematic of the initial conditions considered, in which an internal gravity wave packet (attenuated in  $y$ ) is incident on a horizontal shear layer in a linearly stratified fluid. Red and blue shading indicates the background velocity associated with the horizontal shear  $\mathbf{u}_S$ .

and  $s$  is the wave amplitude that is necessarily less than or equal to unity for a density field that is everywhere statically stable. To maximally favor instability and turbulent transition instigated by the wave-shear interaction, we will henceforth consider a wave of amplitude  $s = 1$ . The wave packet is attenuated over a length scale  $a = 1$ , which is taken to be equivalent to the width of the shear layer. The sign of  $\omega$  is chosen to be positive so that the wave propagates toward the shear layer in the  $y$ -direction when  $k_y > 0$ . Note that the wave vector is nondimensionalized with the shear layer length scale  $L^*$  so that  $\mathbf{k} = \mathbf{k}^* L^*$ ; hence, the components of  $\mathbf{k}$  constitute three additional free dimensionless parameters in the system. A schematic showing the initial conditions for a wave with  $\mathbf{k} = (-1, 1, 4)$  is shown in Figure 1.

## 2.2. Linear theory

The system described by Eqs. (2.1)–(2.3) with initial conditions given by Eq. (2.6) is characterized by a vast parameter space  $\{Ri, Re, Pr, k_x, k_y, k_z\}$ , despite having fixed the wave amplitude  $s = 1$  and attenuation length scale  $a = 1$ . To simplify matters, we begin by describing the linear limiting behaviors of the system in terms of fundamental wave-shear interactions leading to energy growth of the imposed wave perturbations. Depending on the system parameters, the wave can (i) progressively steepen and become trapped within the shear layer and/or (ii) enhance the energy of streamwise perturbations, mechanisms both influencing the resulting generation of turbulence.

We first consider wave trapping. The effect of the horizontal shear flow is to Doppler shift the wave frequency measured by a stationary observer: This is the extrinsic frequency  $\Omega = \omega + u_S k_x$ . Under the assumption  $|k_y| \gg 1$  (i.e., the wavelength in the cross-shear direction is large compared to the shear layer width), WKB theory can be applied to predict the evolution of  $k_y$  along a ray following the wave packet's group velocity

$$\frac{dk_y}{dt} = -k_x \frac{du_S}{dy}, \quad (2.7)$$

where  $d/dt = \partial/\partial t + (\mathbf{c}_g + \mathbf{u}_S) \cdot \nabla$ , and  $\mathbf{c}_g$  is the intrinsic group velocity. It may also be shown that  $k_x, k_z$  and the extrinsic frequency  $\Omega$  are constant along rays (e.g., see Suther-

land 2010). Wave trapping can then occur at a trapping level  $y_t$  determined implicitly in the WKB approximation by equating the initial value of  $\Omega$  with its value at the trapping location

$$u_S(y_t) = \left( \omega(t=0) - Ri^{1/2} \right) / k_x - 1, \quad (2.8)$$

where the wave is assumed to start from the left of the shear layer where  $u_S \approx -1$  (see Figure 1). For a given  $k_y$  and  $k_z$ , the wave is theoretically trapped when Eq. (2.8) has a solution. Since  $-1 < u_S(y_t) < 1$ , this requires  $k_x < 0$  and

$$0 < \frac{\omega(t=0) - Ri^{1/2}}{k_x} < 2 \implies R = \frac{Ri^{1/2}}{2|k_x|} \left( 1 - \frac{\sqrt{k_x^2 + k_y^2}}{|\mathbf{k}|} \right) < 1. \quad (2.9)$$

In dimensional terms, Eq. (2.9) is equivalent to  $R = (N^* - \omega^*) / |2U^*k_x^*| < 1$ , meaning that the difference between the wave frequency and buoyancy frequency is sufficiently small compared to the maximum Doppler shift  $2U^*k_x^*$ . When  $R \ll 1$ , the wave is trapped almost instantly as it enters the shear layer. Notably, prior to trapping, Eq. (2.7) predicts a steepening of the wave in  $y$ , which is found to strongly influence the resulting turbulence.

Independent of Doppler shifting, the wave also acts to advect streamwise ( $u$ ) momentum across the shear layer. In the limit  $k_x \rightarrow 0$ , linearizing the inviscid equations by taking the wave to be a small perturbation to the background flow  $u_S(y)$  yields the  $x$ -momentum equation

$$\frac{\partial u}{\partial t} = -v \frac{\partial u_S}{\partial y}, \quad (2.10)$$

from which it can be seen that perturbation streamwise kinetic energy increases due to advection of the shear layer momentum by the spanwise ( $v$ ) component of the internal wave. This is analogous to the classical lift-up mechanism of Ellingsen & Palm (1975). In our orientation, the lift-up mechanism acts to enhance local vertical shear of streamwise velocity within the horizontal shear layer.

In the case of an unbounded shear layer, the linear evolution of the system was studied in detail by Bakas & Farrell (2009*a,b*), who found that lift-up and wave-trapping mechanisms can create shear-unstable or convectively unstable conditions leading to wave-breaking and turbulence. Wave trapping in a horizontal shear layer similar to that studied here was investigated by Staquet & Huerre (2002), who provided a detailed account of the energetics. Here, we explore a much broader parameter space by systematically varying the parameters  $R$  and  $Ri$  [see Eq. (2.9)] in order to study the differences in non-linear evolution and turbulent transition between the limiting linear growth mechanisms corresponding to wave trapping and lift-up.

### 2.3. Direct numerical simulations

Eight direct numerical simulations (DNS) were performed at fixed values of  $Re = 3500$  and  $Pr = 1$ , for varying values of the wave-trapping parameter  $R$  (controlled through  $k_x$ ) and shear layer Richardson number  $Ri$ , as detailed in Table 1. For simplicity, we fixed  $k_y = 1$  and  $k_z = 4$ . Calculations were performed using the multi-parallel pseudo-spectral channel flow solver DIABLO (Taylor 2008), which employs a second-order finite difference discretization in the wall-bounded ( $y$ ) direction. Time marching is done using a third-order mixed implicit/explicit Runge-Kutta/Crank-Nicolson scheme, and a 2/3 dealiasing rule is applied to the nonlinear terms. Each DNS was performed with  $(N_x, N_y, N_z) = (768, 673, 384)$  grid points, with the resolution chosen such that the grid size was never

Run	$k_x$	$Ri$	$R$	Trapping level ( $y_t$ )
1	-1	1	0.34	$y_t = -0.35$
2	-0.5	1	0.73	$y_t = 0.5$
3	0	1	$\infty$	N/A
4	-1	5	0.75	$y_t = 0.54$
5	-0.5	5	1.64	N/A
6	0	5	$\infty$	N/A
7	-1	0.2	0.15	$y_t = -0.87$
8	0	0.2	$\infty$	N/A

TABLE 1. Dimensionless parameters describing the eight DNS performed, including the trapping level of the wave (if it exists) predicted by WKB theory [Eq. (2.8)].

more than 2.5 times the Kolmogorov length scale. Free-slip/no-flux boundary conditions were applied at  $y = \pm 2\pi$  ( $v = p = 0$ ,  $\partial\phi/\partial y = 0$  for  $\phi = u, w, b$ ), with a sponge layer employed in a region of unit width next to the boundaries within which perturbations were damped to zero quadratically.

### 3. Results

#### 3.1. Phenomenology

To illustrate differences in turbulence production between the wave-trapping and lift-up mechanisms discussed in Section 2.2, slices in the  $yz$ -plane (see Figure 1) at various times for runs 1, 2 and 3 at  $Ri = 1$  are shown in Figure 2. This subset of simulations spans both mechanisms: Run 3 ( $k_x = 0$ ) is purely influenced by lift-up, while runs 2 ( $k_x = -0.5$ ) and 1 ( $k_x = -1$ ) are increasingly affected by wave trapping.

Run 1 [Figures 2(a-d)] has a theoretical trapping level at  $y_t = -0.35$ , reached before the wave encounters maximal shear. While the approximation  $k_y \gg 1$  formally employed by WKB theory is not satisfied by the initial wave packet, the predicted trapping level is found to be a reasonable indicator of the location of energy perturbation growth. Particularly apparent is the steepening of the wave contours in the vicinity of  $y_t$ , which subsequently roll over the trapping line and advect streamwise momentum ( $u$ ) across the shear layer [Figure 2(c)], thus generating substantial vertical shear. This combination of static instability and advection of streamwise momentum results in turbulence production and a rapid cascade of kinetic and potential energy to small scales, followed by a period of decaying turbulence [Figure 2(d)].

In contrast to run 1, run 3 [Figures 2(i-l)] is characterized by  $k_x = 0$ , which precludes Doppler shifting and subsequent wave trapping. Instead, the wave now passes directly through the shear layer [Figure 2(j)] generating strong growth in streamwise velocity perturbations  $u' = u - \bar{u}$  (where  $\bar{u} = \frac{1}{L_x L_z} \int_{-2\pi}^{2\pi} \int_0^{2\pi} u dx dz$ ), as predicted by Eq. (2.10). The resulting vertical shear is sufficiently strong compared with the background stratification to destabilize the flow, with secondary instabilities [Figure 2(k)] eventually leading to the formation of turbulence and small-scale motions [Figure 2(l)]. The structure of the resulting turbulent state is characteristically different to that produced by wave trapping (run 1), with turbulence in run 3 confined to the interfaces between vertical shear

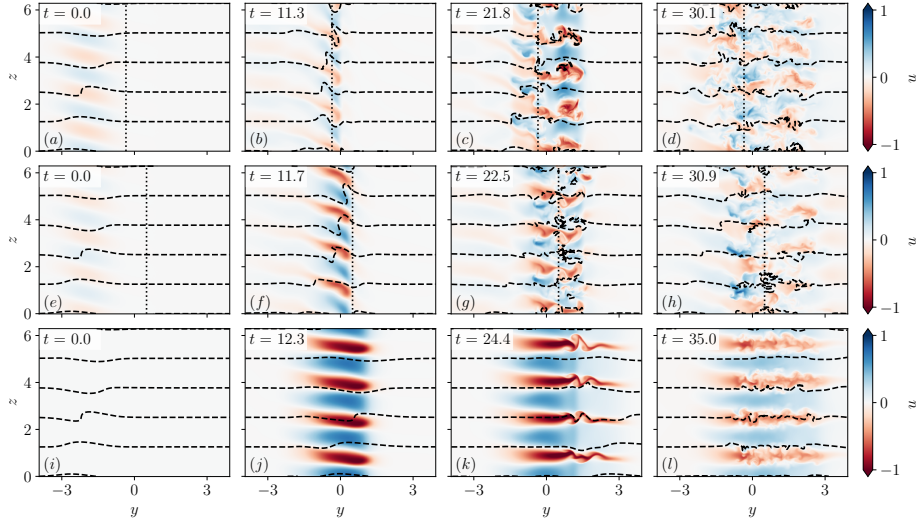


FIGURE 2. Time-evolving vertical snapshots (left to right) in the plane  $x = 0$  of the perturbation streamwise (into the page) velocity field  $u' = u - \bar{u}$  for runs 1 (top row), 2 (middle row) and 3 (bottom row). The center of the shear layer is located at  $y = 0$ . Dashed lines are equispaced constant density isopycnals (isopycnals). Vertical dotted lines in the top two rows show the location of the trapping plane predicted by WKB theory [Eq. (2.9)].

layers, whose length scale is set by the initial wave. Notably, isopycnal displacement due to turbulence is considerably reduced compared with run 1, indicating smaller buoyancy perturbations and less vertical mixing, as will be further considered in Section 3.2.

Finally, run 2 ( $k_x = -0.5$ ) has a somewhat intermediate evolution compared with runs 1 and 3. Wave trapping is predicted to occur further across the shear layer than in run 1, at a location of  $y_t = 0.5$ . As a result, the wave has a longer time to advect momentum across the center of the shear layer in the manner predicted by the lift-up mechanism, leading to the enhanced streamwise velocity perturbations seen in Figure 2(f). Despite the apparent influence of the lift-up mechanism in enhancing vertical shear, however, wave trapping still plays a role, leading to static instability in the density field and the eventual penetration of velocity and density perturbations across the trapping level, analogous to run 1. The resulting turbulent transition shown in Figures 2(g, h) is qualitatively more similar to run 1 than to run 3.

### 3.2. Energetics and mixing

We now more closely consider how the wave-trapping and lift-up mechanisms influence the energy pathways leading to distinct turbulent states. In Figures 3(a–c), we plot domain averages of the available potential energy (APE)  $E_{\text{APE}} = (Ri/2) b'^2$  and squared vertical shear  $\mathcal{S}^2 = (\partial u/\partial z)^2 + (\partial v/\partial z)^2$ , as a function of time  $t$  for runs 1 to 3. Figures 3(d–f) show the corresponding domain-averaged dissipation rates of turbulent kinetic energy ( $\epsilon$ ) and scalar variance ( $\chi$ )

$$\epsilon = (2/Re) s'_{ij} s'_{ij}, \quad \text{where } s'_{ij} = (1/2) (\partial u'_i/\partial x_j + \partial u'_j/\partial x_i), \quad (3.1)$$

$$\chi = (Ri/Re) \nabla b' \cdot \nabla b'. \quad (3.2)$$

To isolate the turbulent state from the dynamics of the initial (non-turbulent) propagation of the wave into the shear layer, the perturbative quantities in the definitions  $\epsilon$

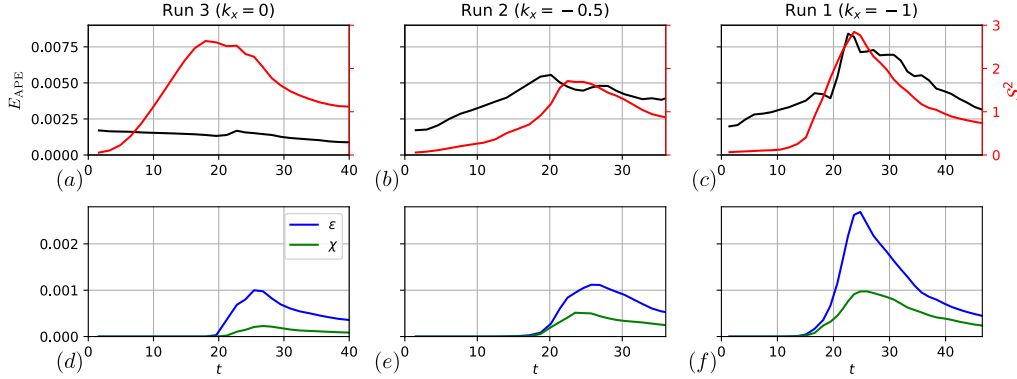


FIGURE 3. Temporal evolution of the domain-averaged available potential energy ( $E_{\text{APE}}$ ), squared vertical shear ( $S^2$ ) and dissipation rates of kinetic ( $\epsilon$ ) and potential ( $\chi$ ) energy for runs 1 to 3 in Figure 2.

and  $\chi$  in Eqs. (3.1) and (3.2) were calculated by subtracting the mean flow aligned with phase lines of the wave, oriented at an angle

$$\theta = \arctan(-k_x/k_z). \quad (3.3)$$

The interplay between the initial buildup of APE (controlled by wave trapping through  $k_x$  at fixed  $Ri$ ) and the generation of vertical shear due to the advection of streamwise ( $u$ ) momentum across the shear layer (controlled by both the convective breaking of the trapped wave and the lift-up mechanism) strongly influences the resulting dissipation rates. When there is no wave trapping (run 3), although strong vertical shear is generated by the lift-up mechanism, the lack of APE buildup results in relatively weak dissipation rates. Conversely, run 1 exhibits relatively strong dissipation rates due to the substantial buildup of both APE and vertical shear.

To study energy exchanges between the wave, shear flow and turbulence, we compute the evolution of the turbulent kinetic energy (TKE) given by

$$\begin{aligned} \underbrace{\frac{\partial}{\partial t} \left( \frac{1}{2} \overline{u'_i u'_i} \right)}_{\partial k / \partial t} + \underbrace{\bar{u}_j \frac{\partial}{\partial x_j} \left( \frac{1}{2} \overline{u'_i u'_i} \right)}_A + \underbrace{\frac{\partial}{\partial x_j} \left( \frac{1}{2} \overline{u'_i u'_i u'_j} \right)}_T = \underbrace{-\overline{u'_i u'_j} \frac{\partial \bar{u}_i}{\partial x_j}}_{P_{ij}} - \underbrace{\frac{\partial}{\partial x_i} \left( \overline{u'_i p'} \right)}_{\Pi} \\ + \frac{1}{\text{Re}_0} \left[ \underbrace{\frac{\partial^2}{\partial x_j \partial x_j} \left( \frac{1}{2} \overline{u'_i u'_i} \right)}_D - \underbrace{2 \overline{s'_{ij} s'_{ij}}}_{\epsilon} + \underbrace{\frac{\partial u'_i}{\partial x_j} \frac{\partial u'_j}{\partial x_i}}_{\mathcal{B}} \right] - \underbrace{\text{Ri} \overline{u'_i \rho'} \delta_{i3}}_B. \quad (3.4) \end{aligned}$$

Here,  $\partial k / \partial t$  denotes the tendency term,  $A$  is advection by the mean flow,  $T$  is turbulent transport,  $P_{ij}$  is the  $[i, j]$  shear production component,  $\Pi$  is pressure transport,  $D$  is viscous diffusion,  $\epsilon$  is the dissipation rate and  $\mathcal{B}$  is the buoyancy flux. As in Figures 3(d–f), quantities in Eq. (3.4) were calculated based on flow variables rotated by the phase angle in Eq. (3.3), to focus solely on the turbulent state. Note that fluctuations based on this definition still include wave variations in  $y$ , and overbars denote ensemble averaging in the along-phase direction.

Figure 4 illustrates the dominant terms in the volume-averaged TKE budget for runs 1 and 3, which exhibited strong convective overturning and enhancement of vertical shear, respectively, as discussed in Section 3.1. An advantage of using a coordinate system

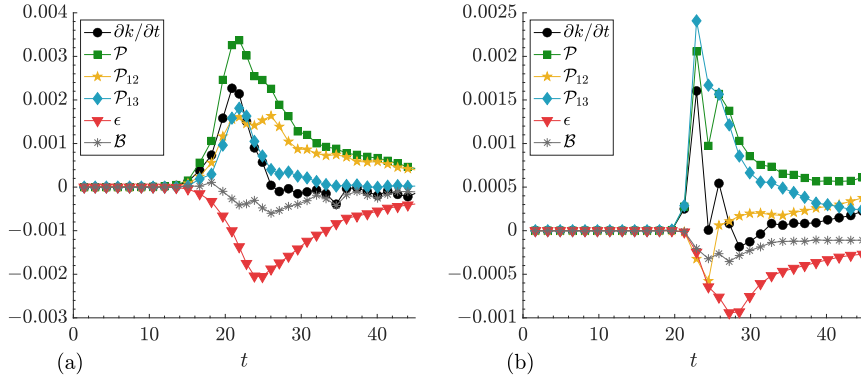


FIGURE 4. Domain-averaged turbulent kinetic energy budgets for (a) run 1 and (b) run 3 with respect to along-phase and across-phase coordinates of the wave. The along-phase direction is treated as the homogeneous coordinate. All quantities are defined in Eq. (3.4).

rotated along wave phase lines is that it more clearly demarcates the onset of turbulence at  $t \approx 15$  in either regime. For run 1 (convective), TKE generation primarily arises from an equal contribution from horizontal (along-phase) and vertical (phase-normal) shear production. The growth in TKE is largely balanced by dissipation with a small additional drain in TKE by negative buoyancy flux  $\mathcal{B}$  converting TKE into turbulent potential energy. The energetic pathway associated with run 3 (lift-up) is quite different in that production is now dominated solely by phase-normal shear. In fact, the turbulence is attenuated by negative along-phase shear production, indicating that energy is being transferred back into the wave. Here as well,  $\mathcal{B}$  acts to transfer kinetic energy to potential.

Note that the peak production for the convective case (run 1) is nearly double that of the lift-up case (run 3) regime on account of wave trapping augmenting the APE reservoir leading to more vigorous turbulence upon wave breaking. This wave-trapping mechanism leads to higher bulk dissipation rates across  $Ri$  as will be discussed in the subsequent section. A future analysis of the mean kinetic and potential energy budgets in this rotated frame may provide further insight into the wave-turbulence coupling.

### 3.3. Influence of the Richardson number

The analyses in Sections 3.1 and 3.2 focused on runs with fixed Richardson number  $Ri = 1$  to highlight key differences between the wave-trapping and lift-up mechanisms that act as precursors to turbulence in this system. We now discuss briefly how these mechanisms change with variable  $Ri$ . The total energy per unit volume of the (infinite) plane wave defined in Eq. (2.6) is

$$E_{wave} = \frac{1}{32\pi^3} \int_0^{2\pi} \int_{-2\pi}^{2\pi} \int_{-2\pi}^{2\pi} \left( \frac{1}{2} |\mathbf{u}_{IW}|^2 + \frac{1}{2} Ri b_{IW}^2 \right) dx dy dz = \frac{s^2 Ri}{2k_z^2}, \quad (3.5)$$

which may be shown to be split evenly between kinetic and potential energy. Similarly, the energy per unit volume in the shear layer may be computed to be

$$E_{shear} = 1 - 2 \tanh(2\pi)/(4\pi) \approx 1. \quad (3.6)$$

For a fixed  $\mathbf{k}$  (and  $s$ ), the total energy of the system increases as  $Ri$  increases. In the wave-trapping scenario, convective motions driven by density overturns may make this additional energy directly available to turbulence [though we note Eq. (2.9) also reveals

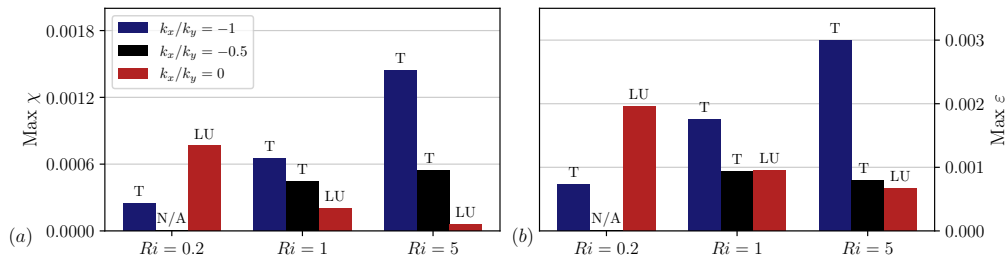


FIGURE 5. Maximum volume-integrated dissipation rates of kinetic energy ( $\epsilon$ , right panel) and scalar variance ( $\chi$ , left panel) for the streamwise wave number  $k_x$  and Richardson number  $Ri$  parameter space spanned by the simulations in Table 1.

that increasing  $Ri$  will eventually lead to  $R > 1$  and hence preclude wave trapping altogether]. However, in the alternative case of lift-up, the vertical shear growth from momentum advection is limited by the velocity difference across the horizontal shear layer. Therefore, for sufficiently large  $Ri$ , the stratification will completely suppress any potential subsequent vertical shear instability.

These general predictions are consistent with the results shown in Figure 5 for  $Ri = \{0.2, 1, 5\}$ , where maximum volume-integrated dissipation rates of turbulent kinetic and available potential energy  $\epsilon$  and  $\chi$  are plotted for each simulation listed in Table 1. In general, runs in which wave trapping occurs (labeled T) exhibit an increase in turbulent dissipation with increasing  $Ri$ , whereas simulations with no wave trapping (labelled LU for lift-up) exhibit the opposite trend. This is a key energetic distinction between the two mechanisms for turbulent transition and supports the argument for characterizing the resulting turbulent states as being convectively versus shear driven. Note that run 5 ( $Ri = 5$ ,  $k_x = -0.5$ ) was not predicted to be trapped by the linear WKB theory, but still exhibits (albeit weaker) wave breaking due to nonlinear amplitude growth from the interaction with the shear (hence, this case is labelled T\*).

#### 4. Conclusions

Using a series of direct numerical simulations, we demonstrated distinct turbulent transition pathways induced by the interaction of an internal wave packet with a horizontal shear layer in a stratified fluid. Linear theory indicates the role of two fundamental wave-shear interactions that serve as mechanisms for energy perturbation growth leading to turbulence, termed here wave trapping and lift-up. Wave trapping, due to the Doppler shifting of the wave frequency by the shear, leads to wave steepening and convective breaking across the shear layer, while lift-up enhances vertical shear purely from the advection of streamwise momentum across the shear layer. An analysis of turbulent statistics and kinetic energy budgets revealed characteristic differences in the turbulent state produced by each mechanism, which were attributed to the variable importance of vertical shear and convective motions caused by the release of available potential energy.

Our results have significant implications for ocean mixing models, where typical sub-grid parameterizations assume a model for turbulence production based solely on vertical shear (e.g. Gregg *et al.* 2018). The observation that energy dissipation rates  $\epsilon$  and  $\chi$  increase with  $Ri$  for wave trapping is counter to the vertical shear paradigm in which increasing  $Ri$  renders the flow increasingly stable to shear instability and hence suppresses turbulence, as was indeed observed for cases dominated purely by the lift-up mechanism.

This finding is, in some sense, a natural consequence of the fact that wave amplitude and energy increase with increasing  $Ri$  in our nondimensionalization. However, it is crucially important to recognize that the pathway to turbulence in this strongly stratified limit is only accessible by convective motions facilitated by wave trapping, driving characteristically different mixing. A more detailed study of the energy exchanges between the wave, shear flow and turbulence, and their dependence on the parameters  $R$  (Eq. [2.9]) and  $Ri$ , is warranted to better understand the interplay between shear and convection in turbulence production. Finally, though our choice of flow parameters spans both wave-trapping and lift-up mechanisms over a range of  $Ri$ , a larger region of parameter space associated with variable  $k_y$  and  $k_z$  remains to be explored.

#### Acknowledgements

We thank L. Thomas, J. Koseff and A. Kaminski for stimulating discussions and suggestions. Support from the CTR program is gratefully acknowledged and MMPC acknowledges additional support from the Natural Sciences and Engineering Research Council of Canada (NSERC) through RGPIN-2024-06184.

#### REFERENCES

- BAKAS, N. A. & FARRELL, B. F. 2009*a* Gravity waves in a horizontal shear flow. Part I: Growth mechanisms in the absence of potential vorticity perturbations. *J. Phys. Oceanogr.* **39**, 481–496.
- BAKAS, N. A. & FARRELL, B. F. 2009*b* Gravity waves in a horizontal shear flow. Part II: Interaction between gravity waves and potential vorticity perturbations. *J. Phys. Oceanogr.* **39**, 497–511.
- BOOKER, J. R. & BRETHERTON, F. P. 1967 The critical layer for internal gravity waves in a shear flow. *J. Fluid Mech.* **27**, 513–539.
- ELLINGSEN, T. & PALM, E. 1975 Stability of linear flow. *Phys. Fluids* **18**, 487–488.
- GARRETT, C. & MUNK, W. 1979 Internal waves in the ocean. *Annu. Rev. Fluid Mech.* **11**, 339–369.
- GREGG, M., D’ASARO, E., RILEY, J. & KUNZE, E. 2018 Mixing efficiency in the ocean. *Annu. Rev. Marine Sci.* **10**, 443–473.
- HOWARD, L. 1961 Note on a paper of John W. Miles. *J. Fluid Mech.* **10**, 509–512.
- JACOBITZ, F. G. & SARKAR, S. 1998 The effect of nonvertical shear on turbulence in a stably stratified medium. *Phys. Fluids* **10**, 1158–1168.
- LEWIN, S. F. & CAULFIELD, C. P. 2024 Evidence for layered anisotropic stratified turbulence in a freely evolving horizontal shear flow. *J. Fluid Mech.* **983**, A20.
- MILES, J. 1961 On the instability of heterogeneous shear flows. *J. Fluid Mech.* **10**, 496–508.
- STAQUET, C. & HUERRE, G. 2002 On transport across a barotropic shear flow by breaking inertia-gravity waves. *Phys. Fluids* **14**, 1993–2006.
- SUTHERLAND, B. R. 2010 *Internal Gravity Waves*. Cambridge University Press.
- TAYLOR, J. 2008 *Numerical simulations of the stratified oceanic bottom layer*. Ph.D. Thesis. University of California, San Diego.
- WATERHOUSE, A. *et al.* 2014 Global patterns of diapycnal mixing from measurements of the turbulent dissipation rate. *J. Phys. Oceanogr.* **44**, 1854–1872.